

J-TETA: Jurnal Teknik Terapan

e-ISSN: 2829-615X

https://j-teta.polije.ac.id/index.php/publikasi/



Enhancing DSSC Performance through Metal-Doped TiO₂ and Poly-Tannin Dye: A Study on Bandgap Reduction and Photon Absorption

Hardeli¹, Annisa Ade Putri¹, Resi Gusmar Lina¹, Widi Feronika¹, dan Putri Permatasari^{2*}

Sitasi: Hardeli.; Putri, Annisa Ade.; Lina, Resi Gusmar.; Feronika, Widi.; Permatasari, Putri. (2025). Enhancing DSSC Performance through Metal-Doped TiO₂ and Poly-Tannin Dye: A Study on Bandgap Reduction and Photon Absorption. J-TETA: Jurnal Teknik Terapan, V(4) N(1), hlm. 19-29.



Copyright: © 2025 oleh para penulis.

Karya ini dilisensikan di bawah Creative
Commons Attribution-Share Alike 4.0
International License.
(https://creativecommons.org/licenses/b
y-sa/4.0/).

- Department of Chemistry, Padang State University, Padang 25131, Indonesia;
- ² Graduate School of Engineering, Gifu University, Gifu 501-1113, Japan;
- * Correspondence: putri.permatasari.s4@s.gifu-u.ac.jp;

Abstract: Dye-sensitized solar cells (DSSC) are a promising alternative to conventional solar cells by using dye molecules to absorb sunlight and facilitate energy conversion. In this study, tannins were used as the dye. Tannins can be polymerized into poly-tannins, which increases the amount of double bonds and therefore improves photon absorption. Furthermore, this study will also examine how metal doping affects the TiO2 semiconductor to further enhance its performance. The selected dopants—Cu, Fe, and Ag—were tested for their capacity to change the bandgap and increase electron mobility. Experiments showed that metal doping lowered the bandgap of TiO2, resulting in better electron excitation and charge transfer. Under optimum conditions, the combination of poly-tannin dye and TiO2-Ag semiconductor resulted in the highest DSSC efficiency (9.18%). Based on this, it can be concluded that combining metal-doped TiO2 with poly-tannin dyes can greatly improve DSSC performance.

Keywords: DSSC, Photovoltaic Efficiency, Poly-Tannin, Semiconductor Bandgap, TiO₂ Modification.

1. Introduction

The global energy problem is becoming more obvious as fossil fuel supplies decrease, and electricity demand rises [1], [2], [3], [4], [5]. As a result, reliable and sustainable alternative energy sources are required [6], [7], [8], [9], [10], [11]. One possibility is the use of solar energy via solar cells [12], [13], [14], [15], [16], [17], [18]. Solar energy is the most abundant form of energy that is limitless, pollution-free, and continuously available [19], [20], [21], [22], [23].

Solar cells are categorised into three main generations. The first generation consists of single and polycrystalline silicon-based solar cells [24], [25], [26], [27]. The second generation includes thin-film solar cells, while the third generation includes dye-sensitised solar cells (DSSC) [28], [29], [30], [31]. DSSCs offer a solar cell solution that is environmentally friendly, non-toxic, and has a lower production cost compared to silicon-based solar cells [32], [33], [34]. However, the efficiency of DSSCs still needs to be improved to be more competitive with other solar cell technologies [35], [36].

DSSCs have a layered structure consisting of TiO₂ nanocrystal-based semiconductors, dyes, working electrodes, carbon or platinum-based opponent electrodes, and electrolyte solutions that maintain the continuity of redox reactions in the cell [37], [38], [39], [40], [41]. TiO₂ is one of the most used inorganic semiconductors in DSSCs due to its photocatalytic, stable, abundant and low-cost properties [42], [43], [44], [45], [46]. However, with a bandgap of just 3.2 eV, TiO₂ only absorbs about 5% of the solar spectrum, limiting it to the ultraviolet (UV) range [44], [47], [48], [49]. As a result, strategies are needed to improve its absorption efficiency in the visible light spectrum.

Several approaches have been proposed for overcoming this, including changing semiconductor composition and doping with metal atoms. Doping has been proven to lower TiO₂'s bandgap, allowing it to absorb light at longer wavelengths [50], [51], [52]. Furthermore, doping can reduce electron-hole recombination, increasing the device's efficiency [53], [54], [55], [56]. Among them, doping with metals including Cu, Fe, and Ag improves TiO₂'s photocatalytic activity [57], [58], [59], [60], [61]. Cu enhances photocatalytic activity by promoting electron transport. Fe has a lower bandgap than TiO₂, allowing for increased absorption of visible light [62], [63], [64], [65], [66]. Meanwhile, Ag is recognized as a transition dopant that can lower particle size and increase the surface area of TiO₂. It also contributes to the plasmonic effect, which can increase light absorption [67], [68], [69], [70], [71].

In addition to semiconductor optimisation, the use of dyes in DSSCs also plays an important role in improving energy conversion efficiency. Organic dyes are widely used in DSSCs because they are low cost, easy to synthesise, and environmentally friendly [35], [38], [72], [73], [74]. However, organic dyes generally have a smaller light absorption area than synthetic dyes [75], [76]. In this study, tannins were chosen as colourants because they are natural macromolecules containing polyhydroxyphenyl groups, which have the potential to increase light absorption.

To improve their absorption efficiency, tannins can be polymerised using cross-linking agents such as glutaraldehyde, which contains two aldehyde groups and is highly effective in forming poly-tannins. Polymerisation of tannins aims to increase the number of double bonds in their molecules, which is expected to maximise photon uptake and improve the efficiency of DSSCs. Therefore, this research focuses on the use of poly-tanine dyes in DSSCs as well as the effect of semiconductor doping on device efficiency, to obtain more efficient and sustainable solar cells.

2. Research Methodology

This research used various laboratory tools such as beakers, measuring cups, watch glass, round bottom flask, stirring rod, volume pipette, dark bottle, spatula, ultrasonic cleaner, volumetric flask, oven, hot plate, analytical balance, magnetic stirrer, vacuum, pycnometer, Oswald viscometer, funnel, and UV lamp. Analytical instruments used include FTIR spectrophotometer, UV-DRS, and digital multimeter. Materials used include tannin, glutaraldehyde (GA, Merck, \geq 25% in water), filter paper (Whatman No. 1), ITO glass (Sigma-Aldrich, surface resistance ~15 Ω /sq), distilled water, aquabidest (Ikapharmindo, p.a.), formaldehyde 37% (Merck, p.a.), KOH (Merck, \geq 85%, pellets), HCl 36% (Merck, p.a.), indicator paper (Merck universal pH indicator), alcohol 70% (Indo Alcohol), aluminum foil (Reynolds), KI/I₂ (potassium iodide and iodine, Merck, p.a.), polyethylene glycol (PEG 400, Merck), acetonitrile p.a. (Merck, \geq 99.8%), methanol p.a. (Merck, \geq 99.9%), TiO₂ Degussa P-25 (Evonik, anatase/rutile ~70:30), FeSO₄·7H₂O (Merck, p.a.), and carbon from wax (locally synthesized from paraffin candle wax via pyrolysis).

Tannin polymerisation was carried out by mixing 36% HCl and 37% formaldehyde solution with tannin, then stirring at 200°C for 2 hours using a magnetic stirrer. The tannin-formaldehyde resin product was filtered, washed with water, and dried in an oven at 80°C. The resin was then dissolved in 2% NaOH solution as initiator and heated at 60-70°C with continuous stirring before adding glutaraldehyde as crosslinker. The polytanin glutaraldehyde resin (PTGR) was then heated at 120°C and cooled to room temperature.

Analysis was carried out before and after polymerisation to see the structural changes between tannins and polytannins. For semiconductor preparation, TiO₂ and FeSO₄.7H₂O were dissolved in methanol and stirred until homogeneous, then sonicated and heated in an oven at 96°C. For Cu-doped TiO₂, TiO₂ was mixed with CuO in methanol, stirred, sonicated, and heated before calcination at 400°C. For Ag-doped TiO₂, PVA was dissolved in distilled water and heated at 80°C while stirring until a suspension was formed, then TiO₂ and AgNO₃ were added and stirred until homogeneous.

In preparation of the DSSC, the ITO glass was cut and cleaned using 70% alcohol in an ultrasonic cleaner. After drying, the resistance of the glass was measured with a multimeter. A layer of scotch tape was attached to the glass, then TiO_2 -doped paste was applied using the doctor blade method and heated at 100° C. The electrolyte solution was made by mixing KI and acetonitrile, then adding I_2 and PEG to form a gel. The counter electrode was made by coating ITO glass with carbon obtained from burning candles.

The dried TiO_2 -doped layer was soaked in poly-tanine dye to allow complete absorption, then dried and arranged with the carbon-based counter electrode in a sandwich structure. The two electrodes were clamped together, and electrolyte solution was dripped between the electrode gaps. The assembled DSSC was tested using a UV lamp with an intensity of 24 W/m², and its efficiency was calculated based on the voltage and current measured using a digital multimeter

3. Results and Discussion

3.1. Dye Preparation

In this study, tannins were used as colourants. Tannins are polyphenolic compounds that have a hydroxyl group (-OH) attached to a benzene ring. These compounds have conjugated double bonds that allow them to absorb photons from the ultraviolet (UV) to visible light spectrum. In this study, tannins were polymerised to increase the number of double bonds.

Firstly, tannins were refluxed with formaldehyde and hydrochloric acid (HCl) at 200°C for 2 hours. A 37% formaldehyde solution is used to dissolve the tannins and facilitate the condensation reaction, as the phenol groups in tannins are highly reactive. Hydrochloric acid acts as an acid catalyst as well as a solvent in this reaction. Formaldehyde acts as a link between tannin monomers by forming methylene bridges (-CH₂), so that the reaction continues with other monomers to form polymers. The reflux process produces a purple-coloured tannin-formaldehyde product.

After refluxing, tannin-formaldehyde was dissolved in NaOH solution and stirred at 70°C for 1 hour. NaOH acts as an initiator that generates free radicals for the polymerisation process and helps to break the double bonds in the crosslinking agent (glutaraldehyde), which will connect the tannin monomers during the polymerisation process. After the addition of NaOH, the initially purple coloured product turned black due to the strong alkaline nature of NaOH. This initiator also affects the chain length of the polymer and increases its molecular weight.

Next, the tannin-formaldehyde mixture was mixed with glutaraldehyde and stirred at 120°C for 90 minutes, resulting in a brown-black poly-tannin precipitate. Glutaraldehyde was chosen as the crosslinking agent because it has two epoxy aldehyde groups, which open during the reaction with NaOH and bind to the tannin-formaldehyde molecules. Increasing the temperature during the addition of glutaraldehyde aims to accelerate the polymerisation reaction rate. The addition of this crosslinking agent increases the number of tannin monomers and double bonds, thereby improving the light absorption ability. The resulting poly-tanine glutaraldehyde resin (PTGR) is then used as a colourant in DSSCs.

3.2. DSSC preparation

The prepared DSSC consists of several components, namely ITO glass substrate, dye, semiconductor, counter electrode, and electrolyte solution. These components are assembled in a sandwich structure. The electrolyte I-/I₂- was applied to both ends of the electrodes, and the voltage generated by the DSSC was measured using a digital multimeter.

Firstly, the ITO glass used as the substrate was cleaned with 70% alcohol to remove impurities and improve its cleanliness. A sonication process was performed for a more optimised cleaning, then the glass was dried and the resistance was measured, with a resistance of 100Ω .

The semiconductor used as a photocatalyst is titanium dioxide (TiO₂ Degussa P-25), which has two phases, 80% anatase and 20% rutile, with an energy gap (bandgap) of 3.27 eV. Doping is done to reduce the bandgap of TiO₂ to increase the efficiency of DSSC, because the smaller the bandgap of a semiconductor, the easier it is for electrons to be excited and move. The metals used in doping are Fe, Ag, and Cu. FeSO₄-7H₂O is used as a precursor for Fe doping, while AgNO₃ and CuO are used for Ag and Cu doping. The sol-gel method was used in the synthesis of TiO₂-doping, in which a phase change occurs from particles dispersed in a liquid (sol) to a macroscopic phase containing liquid (gel). Methanol, as a polar solvent, was used to aid homogenisation and control of metal concentration in the semiconductor synthesis.

In DSSC preparation, TiO_2 -doped semiconductor paste is applied to ITO glass using the doctor blade method and heated at 100° C for 30 minutes to ensure the coating adheres well. After drying, the coating was immersed in polytanine dye so that it could be fully absorbed. The layer that has absorbed the dye is dried again and used as a working electrode in the DSSC.

The carbon counter electrode was made by coating the ITO glass with soot from burning candles. This process is done by passing the glass on the candle flame so that an even layer of black carbon is formed. This carbon layer serves as a catalyst in the electron transfer process.

The electrolytes used are potassium iodide (KI) and iodine (I_2), which act as electron donors for oxidised dye molecules. The electrochemical reaction that occurs is:

$$I^- + I_2 \rightarrow I_3{}^-$$

I ions function as electron donors to return the dye to its initial state and prevent electron recapture. The electrolyte is formulated in semi-solid form with the addition of polyethylene glycol (PEG), which serves to prevent evaporation of the electrolyte solution so that it can be used for a longer period of time. The resulting electrolyte solution

was light yellow in colour and dripped into the gap between the working electrode and the counter electrode. Both electrodes were clamped with clips to ensure the DSSC structure remained stable and did not shift.

DSSC testing was conducted in a box with a 24-watt UV light source. The efficiency of the DSSC was calculated based on the voltage and current measured using a digital multimeter. The working principle of DSSC is that when the dye is exposed to UV light, the electrons in the dye molecule are excited from the HOMO to LUMO energy level. These excited electrons then move to the TiO₂ conduction band, causing oxidation of the dye and producing free electrons. These electrons flow through the ITO glass conductive substrate towards the opposing electrode, generating an electric current in the external circuit. The electrons returning to the cell react with the electrolyte, allowing dye regeneration so that the cycle can repeat.

3.3. Doping Characterization

Characterisation of Ag-doped TiO_2 was performed using UV-Vis DRS spectroscopy to determine the bandgap value of the resulting semiconductor. The addition of Ag metal in the synthesis is expected to reduce the bandgap value of TiO_2 , thereby increasing light absorption in the longer wavelength region. Bandgap is the energy difference between the valence band and the conduction band in a semiconductor material.

The bandgap value is determined using the Tauc Plot method, which estimates the energy gap by plotting the relationship between the absorbed photon energy (hv) on the x-axis and the product of the absorption coefficient with photon energy (αhv)ⁿ on the y-axis. The equation used is:

$$(\alpha h v)^n = K(h v - E_g) \tag{1}$$

where E_8 is the bandgap energy, K is the proportionality constant, and n depends on the type of electronic transition (for anatase TiO₂, n = 2 because the transition is a direct allowed transition).

The absorbance spectrum of TiO_2/Ag obtained through UV-Vis DRS shows a wavelength range between 186-1100 nm. At a wavelength of 304 nm, there is a significant increase in absorbance, which indicates that the $(\alpha hv)^2$ value also increases drastically by 1262.46 (eV cm⁻¹)². This is related to the decrease in transmittance value, where the lower the transmittance, the higher the $(\alpha hv)^2$ value.

Based on the analysis, the bandgap value of pure TiO_2 (anatase phase) is 3.2 eV. After doping with Ag, the bandgap decreased to 2.922 eV, which indicates that Ag doping successfully reduced the semiconductor energy gap. TiO_2/Ag Absorbance and Bandgap of TiO_2/Ag graph using UV-Vis DRS can be seen in Figure 1. This decrease occurs because Ag^+ ions play a role in the charge transfer process from dopant cations to Ti^{4+} ions, which changes the electronic structure and forms lower energy levels.

In addition, the decrease in bandgap can also be attributed to the plasmonic effect of silver (Ag) nanoparticles. This effect increases photon absorption in the visible light range, which is very useful for DSSC applications as it broadens the absorption spectrum of sunlight. However, since the radius of Ag^+ ions is larger (1.15 Å) than that of Ti^{4+} (0.60 Å), only a small part of Ag^+ ions can replace the position of Ti^{4+} in the TiO_2 lattice, so the doping effect may be limited.

The decrease in bandgap obtained in this study indicates a potential increase in DSSC efficiency because it allows electron excitation to occur at lower energies. With a narrower bandgap, TiO₂/Ag can absorb more light in the visible spectrum, thus increasing the number of electrons that can be excited and reducing the recombination rate, which ultimately results in an increase in the energy conversion efficiency of the solar cell.

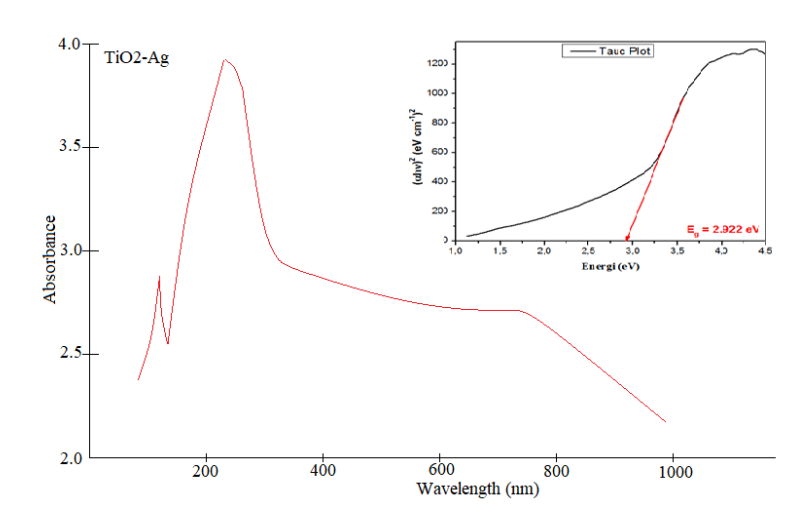


Figure 1. TiO₂/Ag Absorbance and Bandgap of TiO₂/Ag Graph using UV-Vis DRS

Characterisation of CuO-doped TiO_2 was carried out to analyse the change in bandgap energy resulting from the addition of CuO nanoparticles into the TiO_2 matrix. TiO_2 in the anatase phase has a bandgap of 3.2 eV, which causes this material to absorb only about 5% of sunlight, especially in the ultraviolet (UV) spectrum range with wavelengths below 400 nm. Therefore, to increase the photocatalytic activity of TiO_2 , doping with CuO was carried out to expand the light absorption spectrum.

TiO₂/Cu Absorbance Graph using UV-Vis DRS and Bandgap TiO₂/Cu Graph using UV-Vis DRS can be seen in Figure 2. The characterization results showed that after doping with CuO, the bandgap value of TiO₂ dropped to 3.01 eV. The reduction was calculated using the Tauc Plot method using the absorbance value acquired from UV-Vis DRS spectroscopy. CuO doping causes a decrease in bandgap due to the interaction of Cu²⁺ ions with the TiO₂ structure, altering the electrical arrangement in the semiconductor lattice. Cu²⁺ ions, bigger than Ti⁴⁺, can partially replace or occupy interstitial sites in the TiO₂ crystal lattice. This results in the development of new energy levels in the bandgap, which narrows the distance between the valence and conduction bands, thereby improving the material's ability to absorb visible light.

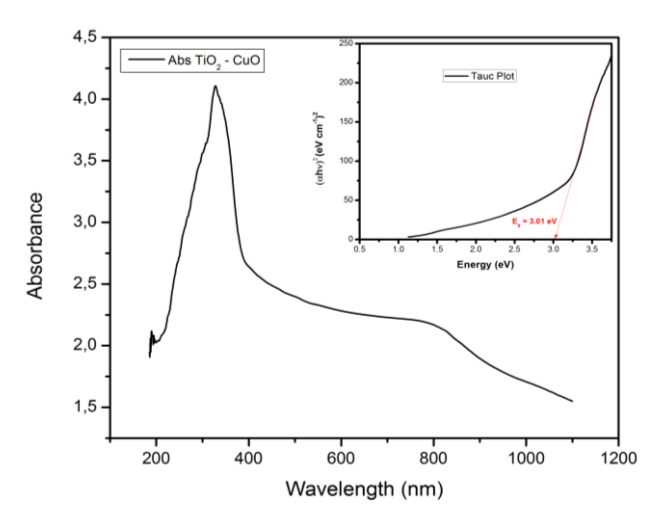


Figure 2. TiO₂/Cu Absorbance Graph using UV-Vis DRS and Bandgap TiO₂/Cu Graph using UV-Vis DRS

CuO doping lowers the bandgap and increases the electrical conductivity of TiO₂. A smaller bandgap allows for electron activation with less photon energy, allowing more electrons to move to the conduction band when exposed to light. As the number of excited electrons increases, the rate of electron-hole recombination decreases, enhancing the photocatalytic efficiency. CuO-doped TiO₂ has a lower bandgap than pure TiO₂, making it more useful for DSSC applications by absorbing more visible light. A reduced bandgap allows more electrons to be excited, improving charge separation and speeding up electron transport in solar cells. This improves DSSCs' energy conversion efficiency, making them more effective in capturing solar energy and converting it into electricity.

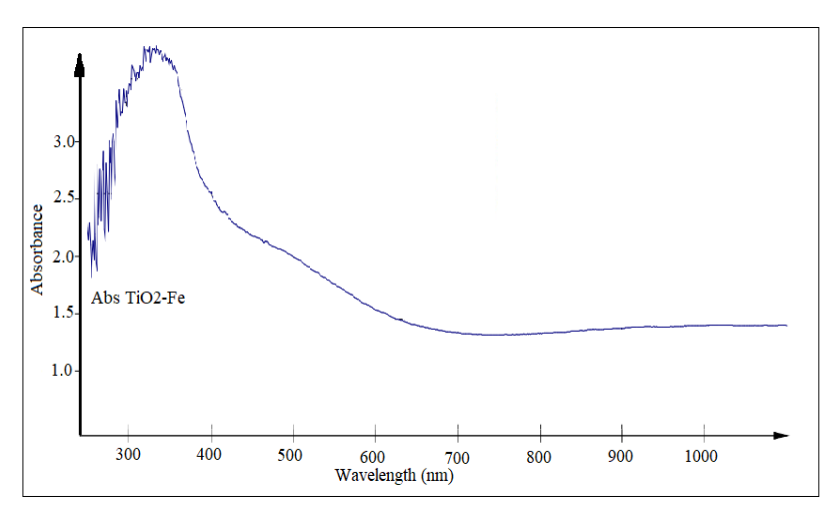


Figure 3. Graph of TiO₂-Fe bandgap values

The graph of TiO₂-Fe bandgap values can be seen in Figure 3. based on the analysis results of the characterization carried out, Fe doping on TiO₂ reduces the band gap from 3.27 eV to 3.05 eV. This decrease is due to the presence of Fe in the TiO₂ structure which forms a metal contact layer. This layer acts as a conductor that accelerates the movement of electrons towards the ITO electrode, thereby increasing the efficiency of charge transfer. Thus, this doping has the potential to increase the efficiency of DSSCs by accelerating electron transport and expanding light absorption to a wider spectrum.

3.4. DSSC Efficiency

Tests were conducted to determine the efficiency of the DSSC based on variations in polymerisation time as well as the effect of tannin monomer concentration in the dye. The efficiency of the DSSC was measured when the cell converted photons into electrical energy with the help of a 24 Watt UV lamp. The efficiency value is obtained by measuring the resistance on the conductive side of the ITO glass and the voltage generated by the cell using a digital multimeter. From the measurement of the resistance and voltage of the DSSC, the electric current produced can be calculated.

DSSC efficiency using pure TiO₂ with tannin and poly-tannin dyes can be seen in Figure 4, while DSSC efficiency using poly-tannin dyes with TiO₂ and doped TiO₂ semiconductors can be seen in Figure 5. The efficiency of the DSSC is calculated using the formula:

$$\eta = \frac{P_{out}}{P_{in}} \times 100\% \tag{2}$$

Where P_{out} is the generated electrical power (V.I), P_{in} is the power from the light source absorbed by the DSSC, and η_i is the energy conversion efficiency. Based on the experimental results, the use of modified dye in DSSC shows an increase in efficiency. Polymerisation of tannins produces molecules with more double bonds, which increases their ability to absorb photons from sunlight. In addition, the prepared dyes were tested on semiconductors that had been modified through doping.

The decrease in the bandgap of the semiconductor contributes to the increase in DSSC efficiency because electron excitation becomes easier with a smaller energy gap. The experimental results show that the highest efficiency of the DSSC obtained is 9.18%, which results from the DSSC with a combination of poly-tanine dye and TiO₂-Ag semiconductor. This shows that the combination of the modified dye and a semiconductor with a lower bandgap provides optimal performance in increasing the efficiency of converting light energy into electricity.

Other parameters that influence DSSC efficiency include the durability of the poly-tanine dye, the effect of Ag doping on electron conductivity, and semiconductor shape. Poly-tanine dyes degrade when exposed to UV light and interact with the electrolyte, which can diminish efficiency over time. Ag doping not only decreases the bandgap, but it also boosts electron mobility, which reduces electron-hole recombination and speeds up charge transfer. Furthermore, the more porous TiO₂-Ag structure can improve the surface area and dye adsorption, resulting in higher efficiency.

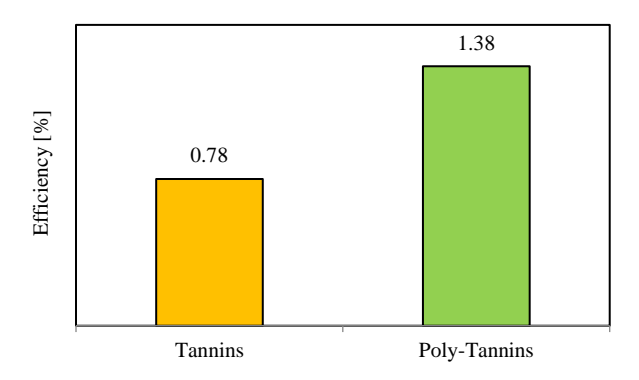


Figure 4. DSSC efficiency using pure TiO2 with tannin and poly-tannin dyes

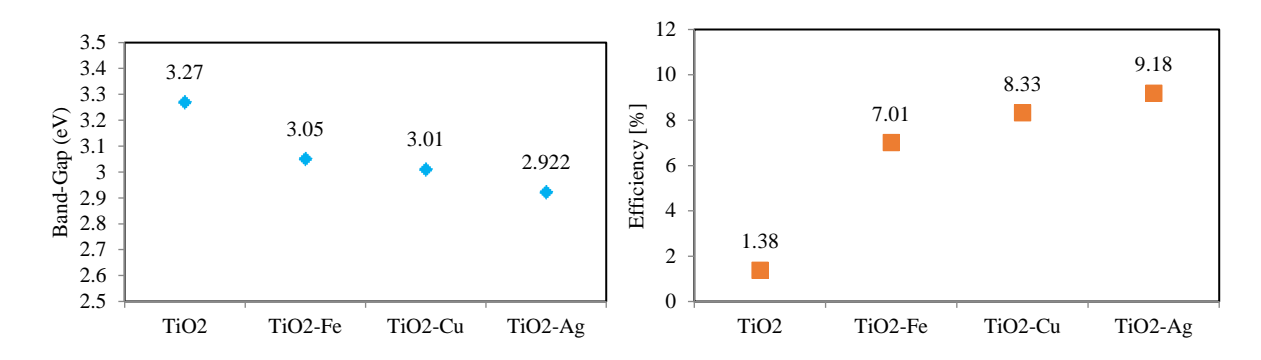


Figure 5. DSSC efficiency using poly-tannin dyes with TiO2 and doped TiO2 semiconductors

4. Conclusion

Due to the presence of more double bonds in the poly-tanine structure, which improves light absorption and energy conversion efficiency, Poly-tanine dyes perform better in DSSCs than pure tannins. Furthermore, it is also known that semiconductors with shorter bandgaps offer higher efficiency, this is because they facilitate electron excitation, which boosts electron mobility in the system. This work reached a maximum efficiency of 9.18% using a DSSC with Ag-doped TiO_2 semiconductor and poly-tanine-based dye. These findings imply that combining metal doping with dye modification can be an effective strategy for improving DSSC performance.

Referensi

- [1] D. Welsby, J. Price, S. Pye, and P. Ekins, "Unextractable fossil fuels in a 1.5 °C world," *Nature*, vol. 597, no. 7875, pp. 230–234, Sep. 2021, doi: 10.1038/s41586-021-03821-8.
- [2] B. P. Resosudarmo, J. F. Rezki, and Y. Effendi, "Prospects of Energy Transition in Indonesia," *Bull Indones Econ Stud*, vol. 59, no. 2, pp. 149–177, May 2023, doi: 10.1080/00074918.2023.2238336.
- [3] A. Raihan, M. I. Pavel, D. A. Muhtasim, S. Farhana, O. Faruk, and A. Paul, "The role of renewable energy use, technological innovation, and forest cover toward green development: Evidence from Indonesia," *Innovation and Green Development*, vol. 2, no. 1, p. 100035, Mar. 2023, doi: 10.1016/j.igd.2023.100035.
- [4] A. Gulagi *et al.*, "Accelerating the transition from coal to renewables in Indonesia to achieve a net-zero energy system," *IET Renewable Power Generation*, vol. 19, no. 1, Jan. 2025, doi: 10.1049/rpg2.13188.
- [5] B. S. Ramadan *et al.*, "Successful energy transition—Case study in Indonesia," in *Decarbonization Strategies and Drivers to Achieve Carbon Neutrality for Sustainability*, Elsevier, 2024, pp. 391–408. doi: 10.1016/B978-0-443-13607-8.00014-6.
- [6] N. Mohammad, W. W. Mohamad Ishak, S. I. Mustapa, and B. V. Ayodele, "Natural Gas as a Key Alternative Energy Source in Sustainable Renewable Energy Transition: A Mini Review," *Front Energy Res*, vol. 9, May 2021, doi: 10.3389/fenrg.2021.625023.
- [7] G. A. Mansoori *et al.*, "Fuels of the Future for Renewable Energy Sources (Ammonia, Biofuels, Hydrogen)," Jan. 2021.

- [8] A. G. Kök, K. Shang, and Ş. Yücel, "Investments in Renewable and Conventional Energy: The Role of Operational Flexibility," *Manufacturing & Service Operations Management*, vol. 22, no. 5, pp. 925–941, Sep. 2020, doi: 10.1287/msom.2019.0789.
- [9] A. G. Kök, K. Shang, and Ş. Yücel, "Investments in Renewable and Conventional Energy: The Role of Operational Flexibility," *Manufacturing & Service Operations Management*, vol. 22, no. 5, pp. 925–941, Sep. 2020, doi: 10.1287/msom.2019.0789.
- [10] M. Höök, J. Li, K. Johansson, and S. Snowden, "Growth Rates of Global Energy Systems and Future Outlooks," *Natural Resources Research*, vol. 21, no. 1, pp. 23–41, Mar. 2012, doi: 10.1007/s11053-011-9162-0.
- [11] B. Podobnik, "Toward a Sustainable Energy Regime," *Technol Forecast Soc Change*, vol. 62, no. 3, pp. 155–172, Nov. 1999, doi: 10.1016/S0040-1625(99)00042-6.
- [12] F. J. M. M. Nijsse *et al.*, "The momentum of the solar energy transition," *Nat Commun*, vol. 14, no. 1, p. 6542, Oct. 2023, doi: 10.1038/s41467-023-41971-7.
- [13] J. Khan and M. H. Arsalan, "Solar power technologies for sustainable electricity generation A review," *Renewable and Sustainable Energy Reviews*, vol. 55, pp. 414–425, Mar. 2016, doi: 10.1016/j.rser.2015.10.135.
- [14] H. H. Pourasl, R. V. Barenji, and V. M. Khojastehnezhad, "Solar energy status in the world: A comprehensive review," *Energy Reports*, vol. 10, pp. 3474–3493, Nov. 2023, doi: 10.1016/j.egyr.2023.10.022.
- [15] M. Shamoushaki and S. C. L. Koh, "Solar cells combined with geothermal or wind power systems reduces climate and environmental impact," *Commun Earth Environ*, vol. 5, no. 1, p. 572, Oct. 2024, doi: 10.1038/s43247-024-01739-3.
- [16] N. Kannan and D. Vakeesan, "Solar energy for future world: A review," *Renewable and Sustainable Energy Reviews*, vol. 62, pp. 1092–1105, Sep. 2016, doi: 10.1016/j.rser.2016.05.022.
- [17] M. Hosenuzzaman, N. A. Rahim, J. Selvaraj, M. Hasanuzzaman, A. B. M. A. Malek, and A. Nahar, "Global prospects, progress, policies, and environmental impact of solar photovoltaic power generation," *Renewable and Sustainable Energy Reviews*, vol. 41, pp. 284–297, Jan. 2015, doi: 10.1016/J.RSER.2014.08.046.
- [18] V. R. Pannase and H. B. Nanavala, "A review of PV technology power generation, PV material, performance and its applications," in 2017 International Conference on Inventive Systems and Control (ICISC), IEEE, Jan. 2017, pp. 1–5. doi: 10.1109/ICISC.2017.8068655.
- [19] Z. Song, M. Wang, and H. Yang, "Quantification of the Impact of Fine Particulate Matter on Solar Energy Resources and Energy Performance of Different Photovoltaic Technologies," *ACS Environmental Au*, vol. 2, no. 3, pp. 275–286, May 2022, doi: 10.1021/acsenvironau.1c00048.
- [20] A. E. Cagle, M. Shepherd, S. M. Grodsky, A. Armstrong, S. M. Jordaan, and R. R. Hernandez, "Standardized metrics to quantify solar energy-land relationships: A global systematic review," *Frontiers in Sustainability*, vol. 3, Feb. 2023, doi: 10.3389/frsus.2022.1035705.
- [21] E. Kabir, P. Kumar, S. Kumar, A. A. Adelodun, and K. H. Kim, "Solar energy: Potential and future prospects," *Renewable and Sustainable Energy Reviews*, vol. 82, pp. 894–900, Feb. 2018, doi: 10.1016/J.RSER.2017.09.094.
- [22] M. K. H. Rabaia *et al.*, "Environmental impacts of solar energy systems: A review," *Science of The Total Environment*, vol. 754, p. 141989, Feb. 2021, doi: 10.1016/J.SCITOTENV.2020.141989.
- [23] S. Ghosh and R. Yadav, "Future of photovoltaic technologies: A comprehensive review," *Sustainable Energy Technologies and Assessments*, vol. 47, p. 101410, Oct. 2021, doi: 10.1016/J.SETA.2021.101410.
- [24] H. Lin *et al.*, "Silicon heterojunction solar cells with up to 26.81% efficiency achieved by electrically optimized nanocrystalline-silicon hole contact layers," *Nat Energy*, vol. 8, no. 8, pp. 789–799, May 2023, doi: 10.1038/s41560-023-01255-2.
- [25] A. S. Subbiah *et al.*, "Efficient blade-coated perovskite/silicon tandems via interface engineering," *Joule*, vol. 9, no. 1, p. 101767, Jan. 2025, doi: 10.1016/j.joule.2024.09.014.
- [26] A. Machín and F. Márquez, "Advancements in Photovoltaic Cell Materials: Silicon, Organic, and Perovskite Solar Cells," *Materials*, vol. 17, no. 5, p. 1165, Mar. 2024, doi: 10.3390/ma17051165.
- [27] W. Liu *et al.*, "Flexible solar cells based on foldable silicon wafers with blunted edges," *Nature*, vol. 617, no. 7962, pp. 717–723, May 2023, doi: 10.1038/s41586-023-05921-z.
- [28] Z. Benzarti and A. Khalfallah, "Recent Advances in the Development of Thin Films," *Coatings*, vol. 14, no. 7, p. 878, Jul. 2024, doi: 10.3390/coatings14070878.

- [29] H. A. Fetouh, A. E. Dissouky, H. A. Salem, M. Fathy, B. Anis, and A. E. Hady Kashyout, "Synthesis, characterization and evaluation of new alternative ruthenium complex for dye sensitized solar cells," *Sci Rep*, vol. 14, no. 1, p. 16718, Jul. 2024, doi: 10.1038/s41598-024-66808-1.
- [30] A. B. Muñoz-García *et al.*, "Dye-sensitized solar cells strike back," *Chem Soc Rev*, vol. 50, no. 22, pp. 12450–12550, 2021, doi: 10.1039/D0CS01336F.
- [31] E. H. Onah, N. L. Lethole, and P. Mukumba, "Luminescent Materials for Dye-Sensitized Solar Cells: Advances and Directions," *Applied Sciences*, vol. 14, no. 20, p. 9202, Oct. 2024, doi: 10.3390/app14209202.
- [32] S. S. Malhotra, M. Ahmed, M. K. Gupta, and A. Ansari, "Metal-free and natural dye-sensitized solar cells: recent advancements and future perspectives," *Sustain Energy Fuels*, vol. 8, no. 18, pp. 4127–4163, 2024, doi: 10.1039/D4SE00406J.
- [33] J. Barichello *et al.*, "Bifacial dye-sensitized solar cells for indoor and outdoor renewable energy-based application," *J Mater Chem C Mater*, vol. 12, no. 7, pp. 2317–2349, 2024, doi: 10.1039/D3TC03220E.
- [34] V. P. Singh and R. Rawat, "The Scope Of Dye-sensitised Solar Cells For Future Applications," *International Journal For Multidisciplinary Research*, vol. 5, no. 5, Oct. 2023, doi: 10.36948/ijfmr.2023.v05i05.7845.
- [35] S. A. Badawy, E. Abdel-Latif, and M. R. Elmorsy, "Tandem dye-sensitized solar cells achieve 12.89% efficiency using novel organic sensitizers," *Sci Rep*, vol. 14, no. 1, p. 26072, Oct. 2024, doi: 10.1038/s41598-024-75959-0.
- [36] C. Hora, F. Santos, M. G. F. Sales, D. Ivanou, and A. Mendes, "Dye-Sensitized Solar Cells for Efficient Solar and Artificial Light Conversion," *ACS Sustain Chem Eng*, vol. 7, no. 15, pp. 13464–13470, Aug. 2019, doi: 10.1021/acssuschemeng.9b02990.
- [37] M. Sibiński *et al.*, "Impact of blocking layers based on TiO₂ and ZnO prepared via direct current reactive magnetron sputtering on DSSC solar cells," *Sci Rep*, vol. 14, no. 1, p. 10676, May 2024, doi: 10.1038/s41598-024-61512-6.
- [38] S. Rahman *et al.*, "Research on dye sensitized solar cells: recent advancement toward the various constituents of dye sensitized solar cells for efficiency enhancement and future prospects," *RSC Adv*, vol. 13, no. 28, pp. 19508–19529, 2023, doi: 10.1039/D3RA00903C.
- [39] S. Ding, C. Yang, J. Yuan, H. Li, X. Yuan, and M. Li, "An overview of the preparation and application of counter electrodes for DSSCs," *RSC Adv*, vol. 13, no. 18, pp. 12309–12319, 2023, doi: 10.1039/D3RA00926B.
- [40] R. Kumar, V. Sahajwalla, and P. Bhargava, "Fabrication of a counter electrode for dye-sensitized solar cells (DSSCs) using a carbon material produced with the organic ligand 2-methyl-8-hydroxyquinolinol (Mq)," *Nanoscale Adv*, vol. 1, no. 8, pp. 3192–3199, 2019, doi: 10.1039/C9NA00206E.
- [41] K. Prajapat *et al.*, "Next-generation counter electrodes for dye-sensitized solar cells: A comprehensive overview," *Sustainable Materials and Technologies*, vol. 42, p. e01178, Dec. 2024, doi: 10.1016/J.SUSMAT.2024.E01178.
- [42] K. V. Srivastava, P. Srivastava, A. Srivastava, R. K. Maurya, Y. P. Singh, and A. Srivastava, "1D TiO₂ photoanodes: a game-changer for high-efficiency dye-sensitized solar cells," *RSC Adv*, vol. 15, no. 7, pp. 4789–4819, 2025, doi: 10.1039/D4RA06254J.
- [43] H. Pu, C. Tian, and H. Zhang, "In situ hydrothermal synthesis of visible light active sulfur doped TiO₂ from industrial TiOSO4 solution," *Sci Rep*, vol. 14, no. 1, p. 31258, Dec. 2024, doi: 10.1038/s41598-024-82640-z.
- [44] N. M. Chauke, R. L. Mohlala, S. Ngqoloda, and M. C. Raphulu, "Harnessing visible light: enhancing TiO₂ photocatalysis with photosensitizers for sustainable and efficient environmental solutions," *Frontiers in Chemical Engineering*, vol. 6, Feb. 2024, doi: 10.3389/fceng.2024.1356021.
- [45] D. Jiang *et al.*, "A Review on Metal Ions Modified TiO₂ for Photocatalytic Degradation of Organic Pollutants," *Catalysts*, vol. 11, no. 9, p. 1039, Aug. 2021, doi: 10.3390/catal11091039.
- [46] S. Borbón, S. Lugo, D. Pourjafari, N. Pineda Aguilar, G. Oskam, and I. López, "Open-Circuit Voltage (VOC) Enhancement in TiO₂-Based DSSCs: Incorporation of ZnO Nanoflowers and Au Nanoparticles," *ACS Omega*, vol. 5, no. 19, pp. 10977–10986, May 2020, doi: 10.1021/acsomega.0c00794.
- [47] M. A. Ibrahem, E. Verrelli, A. M. Adawi, J.-S. G. Bouillard, and M. O'Neill, "Plasmons Enhancing Sub-Bandgap Photoconductivity in TiO₂ Nanoparticles Film," *ACS Omega*, vol. 9, no. 9, pp. 10169–10176, Mar. 2024, doi: 10.1021/acsomega.3c06932.
- [48] E. M. Kutorglo *et al.*, "Efficient full solar spectrum-driven photocatalytic hydrogen production on low bandgap TiO₂/conjugated polymer nanostructures," *RSC Adv*, vol. 13, no. 34, pp. 24038–24052, 2023, doi: 10.1039/D3RA04049F.

- [49] C. Liao, Y. Li, and S. C. Tjong, "Visible-Light Active Titanium Dioxide Nanomaterials with Bactericidal Properties," *Nanomaterials*, vol. 10, no. 1, p. 124, Jan. 2020, doi: 10.3390/nano10010124.
- [50] M. Zhang *et al.*, "Ti3+ Self-Doping of TiO₂ Boosts Its Photocatalytic Performance: A Synergistic Mechanism," *Molecules*, vol. 29, no. 22, p. 5385, Nov. 2024, doi: 10.3390/molecules29225385.
- [51] Y. Taneja, D. Dube, and R. Singh, "Recent advances in elemental doping and simulation techniques: improving structural, photophysical and electronic properties of titanium dioxide," *J Mater Chem C Mater*, vol. 12, no. 37, pp. 14774–14808, 2024, doi: 10.1039/D4TC02031F.
- [52] J. F. Fatriansyah *et al.*, "The Effect of Zn Doping to TiO₂ Thin Film Band Gap and Photocatalytic Performance: Experiment and Density Functional Theory Simulation," in 2023 6th International Seminar on Research of Information Technology and Intelligent Systems (ISRITI), IEEE, Dec. 2023, pp. 324–330. doi: 10.1109/ISRITI60336.2023.10467760.
- [53] N. A. Erfan, M. S. Mahmoud, H. Y. Kim, and N. A. M. Barakat, "Synergistic doping with Ag, CdO, and ZnO to overcome electron-hole recombination in TiO₂ photocatalysis for effective water photo splitting reaction," *Front Chem*, vol. 11, Nov. 2023, doi: 10.3389/fchem.2023.1301172.
- [54] S. Mohammadi, S. Akbari Nia, and D. Abbaszadeh, "Reduction of recombination at the interface of perovskite and electron transport layer with graded pt quantum dot doping in ambient air-processed perovskite solar cell," *Sci Rep*, vol. 14, no. 1, p. 24254, Oct. 2024, doi: 10.1038/s41598-024-75495-x.
- [55] N. A. Erfan, M. S. Mahmoud, H. Y. Kim, and N. A. M. Barakat, "Synergistic doping with Ag, CdO, and ZnO to overcome electron-hole recombination in TiO₂ photocatalysis for effective water photo splitting reaction," *Front Chem*, vol. 11, Nov. 2023, doi: 10.3389/fchem.2023.1301172.
- [56] M. M. Mazumder, M. Akteruzzaman, H. Yeasmin, and R. Islam, "Doping in TiO₂ to improve solar cell efficiency: A Comprehensive Review," Jun. 05, 2023. doi: 10.26434/chemrxiv-2023-ffmq9.
- [57] I. Abdelfattah and A. M. El-Shamy, "A comparative study for optimizing photocatalytic activity of TiO₂-based composites with ZrO₂, ZnO, Ta₂O₅, SnO, Fe₂O₃, and CuO additives," *Sci Rep*, vol. 14, no. 1, p. 27175, Nov. 2024, doi: 10.1038/s41598-024-77752-5.
- [58] A. M. Alotaibi *et al.*, "Enhanced Photocatalytic and Antibacterial Ability of Cu-Doped Anatase TiO 2 Thin Films: Theory and Experiment," *ACS Appl Mater Interfaces*, vol. 12, no. 13, pp. 15348–15361, Apr. 2020, doi: 10.1021/acsami.9b22056.
- [59] T. Tian, J. Zhang, L. Tian, S. Ge, and Z. Zhai, "Photocatalytic Degradation of Gaseous Benzene Using Cu/Fe-Doped TiO₂ Nanocatalysts under Visible Light," *Molecules*, vol. 29, no. 1, p. 144, Dec. 2023, doi: 10.3390/molecules29010144.
- [60] K. H. Lee *et al.*, "The Comparison of Metal Doped TiO₂ Photocatalytic Active Fabrics under Sunlight for Waste Water Treatment Applications," *Catalysts*, vol. 13, no. 9, p. 1293, Sep. 2023, doi: 10.3390/catal13091293.
- [61] A. Khlyustova, N. Sirotkin, T. Kusova, A. Kraev, V. Titov, and A. Agafonov, "Doped TiO₂: the effect of doping elements on photocatalytic activity," *Mater Adv*, vol. 1, no. 5, pp. 1193–1201, 2020, doi: 10.1039/D0MA00171F.
- [62] A. Mancuso *et al.*, "Visible Light-Driven Photocatalytic Activity and Kinetics of Fe-Doped TiO₂ Prepared by a Three-Block Copolymer Templating Approach," *Materials*, vol. 14, no. 11, p. 3105, Jun. 2021, doi: 10.3390/ma14113105.
- [63] X. Feng, Z. Liu, L. Qin, S.-Z. Kang, and X. Li, "Photocatalytic activity and the electron transport mechanism of titanium dioxide microsphere/porphyrin implanted with small size copper," *Physical Chemistry Chemical Physics*, vol. 22, no. 24, pp. 13528–13535, 2020, doi: 10.1039/D0CP01953D.
- [64] N. Wetchakun, P. Pirakitikulr, K. Chiang, and S. Phanichphant, "Visible light-active nano-sized Fe-doped TiO₂ photocatalysts and their characterization," in 2008 2nd IEEE International Nanoelectronics Conference, IEEE, 2008, pp. 836–841. doi: 10.1109/INEC.2008.4585613.
- [65] S. K. Gharaei, M. Abbasnejad, and R. Maezono, "Bandgap reduction of photocatalytic TiO₂ nanotube by Cu doping," *Sci Rep*, vol. 8, no. 1, p. 14192, Sep. 2018, doi: 10.1038/s41598-018-32130-w.
- [66] A. M. Alotaibi *et al.*, "Enhanced Photocatalytic and Antibacterial Ability of Cu-Doped Anatase TiO₂ Thin Films: Theory and Experiment," *ACS Appl Mater Interfaces*, vol. 12, no. 13, pp. 15348–15361, Apr. 2020, doi: 10.1021/acsami.9b22056.

- [67] Y. Cherif *et al.*, "Facile Synthesis of Gram-Scale Mesoporous Ag/TiO₂ Photocatalysts for Pharmaceutical Water Pollutant Removal and Green Hydrogen Generation," *ACS Omega*, vol. 8, no. 1, pp. 1249–1261, Jan. 2023, doi: 10.1021/acsomega.2c06657.
- [68] S. Wanwong, W. Sangkhun, P. Jiamboonsri, and T. Butburee, "Electrospun silk nanofiber loaded with Ag-doped TiO 2 with high-reactive facet as multifunctional air filter," *RSC Adv*, vol. 13, no. 37, pp. 25729–25737, 2023, doi: 10.1039/D3RA04621D.
- [69] S. Kr. Singh, U. Kr. Samanta, A. Dhar, and M. Chandra Paul, "Structural, Morphological, and Optical Properties of Ag-Doped TiO 2 Thin-Film over Fiber Optic Substrate for Sensing Applications," *physica status solidi (a)*, vol. 218, no. 22, Nov. 2021, doi: 10.1002/pssa.202100447.
- [70] S. Arain *et al.*, "Microemulsion-Based Synthesis of Highly Efficient Ag-Doped Fibrous SiO2-TiO2 Photoanodes for Photoelectrochemical Water Splitting," *Catalysts*, vol. 15, no. 1, p. 66, Jan. 2025, doi: 10.3390/catal15010066.
- [71] O. AVCİATA, Y. BENLİ, S. GORDUK, and O. KOYUN, "Ag doped TiO₂ nanoparticles prepared by hydrothermal method and coating of the nanoparticles on the ceramic pellets for photocatalytic study: Surface properties and photoactivity," *Journal of Engineering Technology and Applied Sciences*, vol. 1, no. 1, pp. 34–50, May 2016, doi: 10.30931/jetas.281381.
- [72] A. Zdyb and E. Krawczak, "Organic Dyes in Dye-Sensitized Solar Cells Featuring Back Reflector," *Energies* (*Basel*), vol. 14, no. 17, p. 5529, Sep. 2021, doi: 10.3390/en14175529.
- [73] G. G. Asfaw, N. E. Benti, M. A. Desta, and Y. S. Mekonnen, "Design and fabrication of TiO₂-based dye sensitized solar cells using plant-derived organic dyes," *AIP Adv*, vol. 13, no. 7, Jul. 2023, doi: 10.1063/5.0153639.
- [74] R. H. Kisdina *et al.*, "Characterization of Natural and Synthetic Dyes for Large-Scale Dye-Sensitized Solar Cells," *Defect and Diffusion Forum*, vol. 438, pp. 69–78, Feb. 2025, doi: 10.4028/p-BsQ0OO.
- [75] Basuki, Suyitno, and B. Kristiawan, "Absorbance and electrochemical properties of natural indigo dye," 2018, p. 030067. doi: 10.1063/1.5024126.
- [76] A. Dessì *et al.*, "D–A– π –A organic dyes with tailored green light absorption for potential application in greenhouse-integrated dye-sensitized solar cells," *Sustain Energy Fuels*, vol. 5, no. 4, pp. 1171–1183, 2021, doi: 10.1039/D0SE01610A.